






Atazanavir, Alone or in Combination with Ritonavir, Inhibits SARS-CoV-2 Replication and Proinflammatory Cytokine Production

Natalia Fintelman-Rodrigues,^{a,i} Carolina Q. Sacramento,^{a,i} Carlyle Ribeiro Lima,ⁱ Franklin Souza da Silva,^{b,i} André C. Ferreira,^{a,c,i} Mayara Mattos,^{a,i} Caroline S. de Freitas,^{a,i} Vinicius Cardoso Soares,^a Suelen da Silva Gomes Dias,^a Jairo R. Temerozo,^{d,e}  Milene D. Miranda,^f Aline R. Matos,^f Fernando A. Bozza,^{g,h} Nicolas Carels,ⁱ Carlos Roberto Alves,^b Marilda M. Siqueira,^f  Patrícia T. Bozza,^a  Thiago Moreno L. Souza^{a,i}

^aLaboratório de Imunofarmacologia, Instituto Oswaldo Cruz (IOC), Fundação Oswaldo Cruz (Fiocruz), Rio de Janeiro, Rio de Janeiro, Brazil

^bLaboratório de Biologia Molecular e Doenças Endêmicas, IOC, Fiocruz, Rio de Janeiro, Rio de Janeiro, Brazil

^cUniversidade Iguazu, Nova Iguaçu, Rio de Janeiro, Brazil

^dLaboratório de Pesquisas sobre o Timo, IOC, Fiocruz, Rio de Janeiro, Rio de Janeiro, Brazil

^eNational Institute for Science and Technology on Neuroimmunomodulation (INCT/NIM), IOC, Fiocruz, Rio de Janeiro, Rio de Janeiro, Brazil

^fLaboratório de Vírus Respiratório e do Sarampo, IOC, Fiocruz, Rio de Janeiro, Rio de Janeiro, Brazil

^gInstituto Nacional de Infectologia Evandro Chagas, Fiocruz, Rio de Janeiro, Rio de Janeiro, Brazil

^hInstituto D'or de Pesquisa e Ensino, Rio de Janeiro, Rio de Janeiro, Brazil

ⁱNational Institute for Science and Technology on Innovation in Diseases of Neglected Populations (INCT/IDPN), Center for Technological Development in Health (CDTS), Fiocruz, Rio de Janeiro, Rio de Janeiro, Brazil

Natalia Fintelman-Rodrigues, Carolina Q. Sacramento, and Carlyle Ribeiro Lima contributed equally to this work. The order of the first three authors was determined alphabetically, excluding the first given name.

ABSTRACT Severe acute respiratory syndrome coronavirus 2 (SARS-CoV-2) is already responsible for far more deaths than previous pathogenic coronaviruses (CoVs) from 2002 and 2012. The identification of clinically approved drugs to be repurposed to combat 2019 CoV disease (COVID-19) would allow the rapid implementation of potentially life-saving procedures. The major protease (Mpro) of SARS-CoV-2 is considered a promising target, based on previous results from related CoVs with lopinavir (LPV), an HIV protease inhibitor. However, limited evidence exists for other clinically approved antiretroviral protease inhibitors. Extensive use of atazanavir (ATV) as antiretroviral and previous evidence suggesting its bioavailability within the respiratory tract prompted us to study this molecule against SARS-CoV-2. Our results show that ATV docks in the active site of SARS-CoV-2 Mpro with greater strength than LPV, blocking Mpro activity. We confirmed that ATV inhibits SARS-CoV-2 replication, alone or in combination with ritonavir (RTV) in Vero cells and a human pulmonary epithelial cell line. ATV/RTV also impaired virus-induced enhancement of interleukin 6 (IL-6) and tumor necrosis factor alpha (TNF- α) levels. Together, our data strongly suggest that ATV and ATV/RTV should be considered among the candidate repurposed drugs undergoing clinical trials in the fight against COVID-19.

KEYWORDS COVID-19, SARS-CoV-2, antiviral, atazanavir, coronavirus

Coronaviruses (CoVs) are single-stranded positive-sense RNA viruses able to infect a range of hosts, from animals to humans (1). At the beginning of the 21st century, highly pathogenic CoVs emerged, such as the severe acute respiratory syndrome (SARS-CoV), middle-east respiratory syndrome (MERS-CoV) (2), and, at the end of 2019, a novel variant of SARS-CoV (SARS-CoV-2) (3). SARS-CoV-2 has spilled over to humans from animal reservoirs, most likely bats and/or pangolins (3). Both SARS- and MERS-CoV raised international public health concerns with rates of mortality of 10% and 35%,

Citation Fintelman-Rodrigues N, Sacramento CQ, Ribeiro Lima C, Souza da Silva F, Ferreira AC, Mattos M, de Freitas CS, Cardoso Soares V, da Silva Gomes Dias S, Temerozo JR, Miranda MD, Matos AR, Bozza FA, Carels N, Alves CR, Siqueira MM, Bozza PT, Souza TML. 2020. Atazanavir, alone or in combination with ritonavir, inhibits SARS-CoV-2 replication and proinflammatory cytokine production. *Antimicrob Agents Chemother* 64:e00825-20. <https://doi.org/10.1128/AAC.00825-20>.

Copyright © 2020 American Society for Microbiology. All Rights Reserved.

Address correspondence to Thiago Moreno L. Souza, tmoreno@cdts.fiocruz.br.

Received 28 April 2020

Returned for modification 25 May 2020

Accepted 2 August 2020

Accepted manuscript posted online 5 August 2020

Published 21 September 2020

respectively (4, 5). SARS-CoV-2 became a pandemic threat and provoked 5% to 10% mortality, resulting in more than 600,000 deaths in 7 months (6).

Currently, the most effective response to the SARS-CoV-2 pandemic has been social distancing, to avoid contact between infected and uninfected individuals and flatten the virus dissemination curve. While these social actions can disrupt virus transmission rates, they are not expected to reduce the absolute number of infected individuals. Furthermore, these strategies are also provoking a severe reduction in global economic activity (7). To effectively combat the impact of SARS-CoV-2 on infected individuals, and society as a whole, it is essential to identify antiviral drugs for immediate use as well as develop new drugs and a vaccine for long-term solutions to the disease associated with SARS-CoV-2 (COVID-19).

Repurposing of clinically approved drugs is the fastest pathway to identify therapeutics (8). Some of the most promising antiviral candidates against SARS-CoV-2 have been under investigation since the outbreak of SARS-CoV in 2002. Building on this continuous investigation, an unprecedented effort from the World Health Organization (WHO) to run a global clinical trial, called Solidarity, is ongoing (9). This mega trial has been putting forward lopinavir (LPV)/ritonavir (RTV), in combination or not with beta interferon (IFN- β), chloroquine (CQ), and remdesivir to treat COVID-19 (9). Some of the arms of the Solidarity trial are under reevaluation due to limited clinical benefits of CQ and LPV/RTV (9–11). Thus, other antiviral candidates must be evaluated from a preclinical perspective.

The most successful antiviral drugs often directly target viral enzymes (12). For CoVs, the major protease (Mpro) has been a promising drug target for almost 2 decades, starting with early studies on 2002 SARS-CoV that showed this enzyme to be inhibited by LPV/RTV, inhibitors of HIV protease (13). Mpro is required during the CoV replication cycle to process viral polyprotein (14). Highly pathogenic CoVs contain two open reading frames, ORF1a and ORF1b, that are translated by host ribosomes into their two respective viral polyproteins, pp1a and pp1ab. ORF1a encodes two cysteine proteases, the papain-like protease (PLpro) and Mpro. While PLpro cuts the polyprotein at three sites, Mpro is responsible for cleavage at 11 other locations that, together, produce the 16 nonstructural proteins.

In a combined therapy of LPV with RTV, LPV is included as the principle antiviral compound and RTV as an inhibitor of drug metabolism, being a specific inhibitor of the cytochrome P450, CYP3A4 isoform (15). In the early 2000s, another contemporary antiretroviral protease inhibitor, atazanavir (ATV), replaced LPV due to fewer side effects for the patients (16, 17). Contemporarily, *in silico* evidence suggested that other HIV protease inhibitors would target SARS-CoV-2 Mpro better than LPV, which included ATV (18). Importantly, ATV has been described to reach the lungs after intravenous administration (19, 20). Moreover, a proposed secondary use of ATV to treat pulmonary fibrosis suggested that this drug functionally reaches the lungs (20).

The seriousness of COVID-19 and the need for an immediate oral intervention, along with this series of observations with HIV protease inhibitors, motivated us to evaluate the susceptibility of SARS-CoV-2 to ATV. Since ATV is available as a clinical treatment alone or in combination with RTV, both therapies were studied. For the first time, we describe that SARS-CoV-2 Mpro is a target for ATV, which, alone or with RTV, inhibits viral replication and prevents the release of cytokine storm-associated mediators. Our timely data highlights an additional therapeutic approach against COVID-19 that should be considered for clinical trials with another protease inhibitor, which is superior to LPV *in vitro*.

RESULTS

ATV docks into SARS-CoV-2 Mpro more spontaneously and stably than LPV. SARS-CoV-2 enzyme Mpro (PDB 6LU7) supports docking by both ATV and LPV (see Fig. S1 and S2 in the supplemental material). ATV and LPV occupy S1* and the S2 cleft of their active sites with free energy scores of -59.87 and -65.49 kcal/mol, respectively

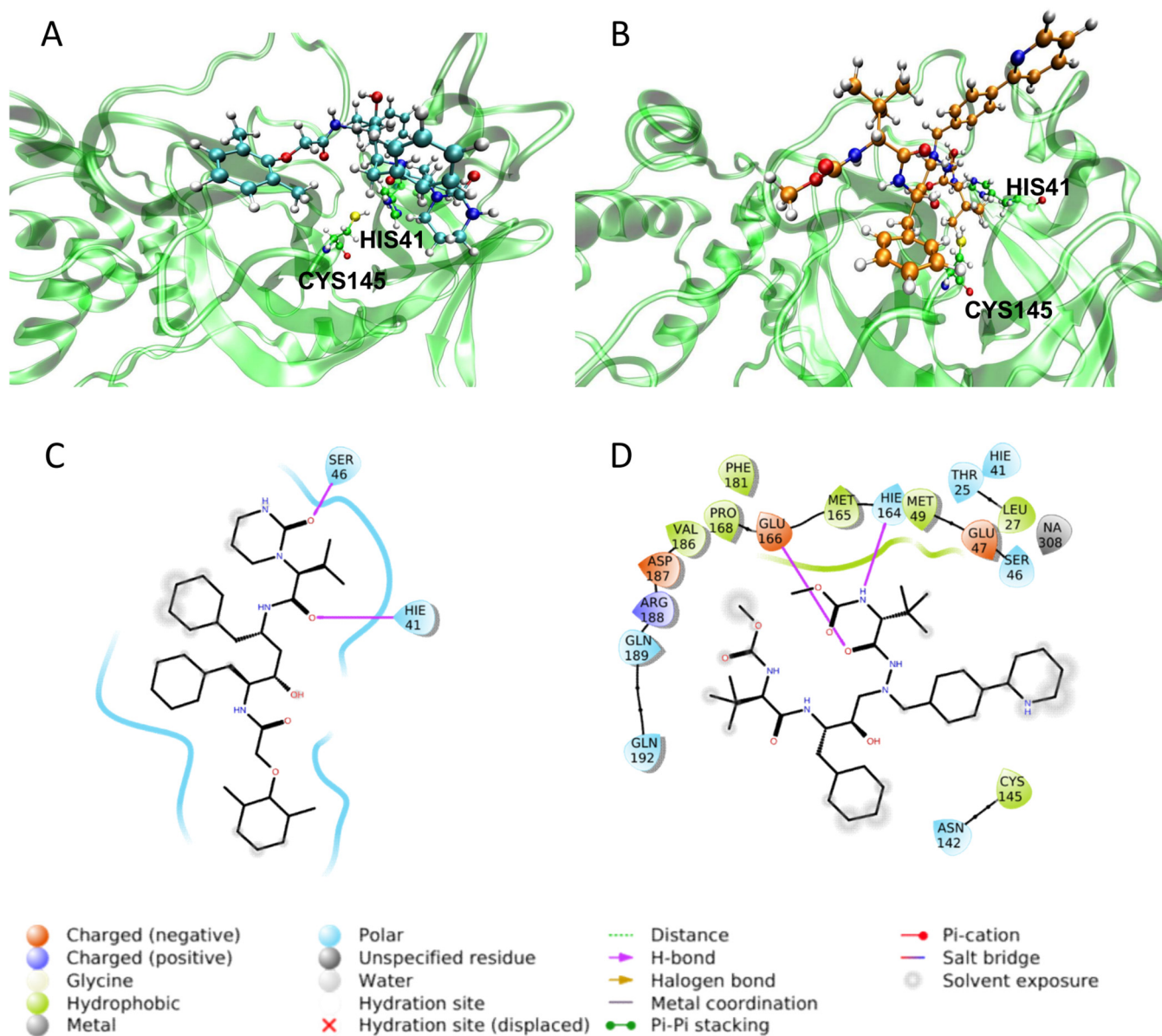


FIG 1 Final positions of ATV and LPV on Mpro at the end of a molecular dynamics simulation. Representative images of LPV (A; blue structure) and ATV (B; orange structure) positioned in Mpro (green). Two-dimensional (2D) representation of the interactions of LPV (C) and ATV (D) in the Mpro active site at the end of 100-ns molecular dynamics simulation.

(Fig. S1 and S2). ATV bound more spontaneously because of its hydrogen bonds with Mpro, whereas LPV depends on hydrophobic interactions (Fig. S2).

Molecular dynamics analysis revealed that the root mean square deviation (RMSD) for the SARS-CoV-2 Mpro backbone presented different conformations in complex with ATV or LPV (see Fig. S3). LPV was initially at a 3.8-Å distance from the catalytic residue Cys145 (see Fig. S4A and S5A). After conformational changes, LPV was 7.17 Å distant from the active site (Fig. 1A and C), likely limiting its antiviral activity. Another critical residue, His41, was satisfactorily at a distance of 2.89 Å from bound LPV (Fig. 1A and C). ATV interacted with neither His41 nor Cys145 at initial analysis (Fig. S4B and S5B). Nevertheless, ATV's position remained stable within the active site independently of conformational changes (Fig. 1B and D). The steric occupation of the cleft in the enzymatic active site by ATV, which blocks the residues of the catalytic amino acids, can be explained by its stronger interactions with Mpro than LPV (Tables S1 to S3).

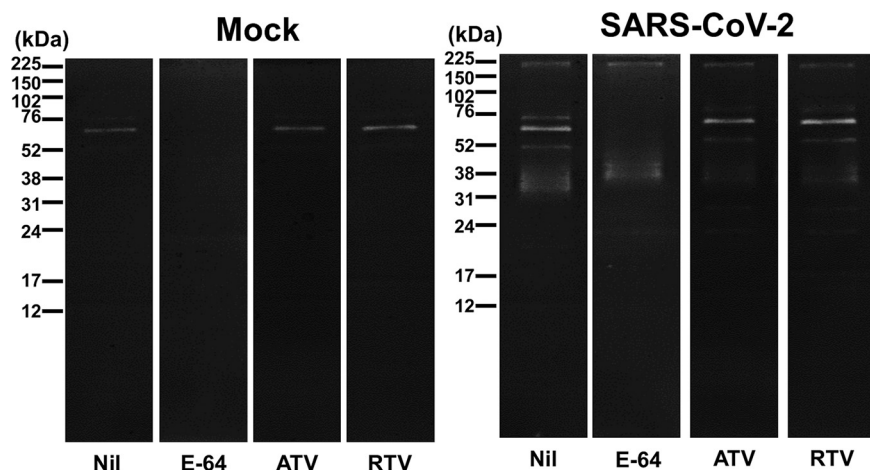


FIG 2 Inhibition of proteinase activity through an analysis of gelatinolytic activity. Vero cells were mock treated or infected with SARS-CoV-2 at an MOI of 0.1 for 48 h before lysis and preparation of a cellular fraction. Fractions containing 12 μg of total protein were separated by electrophoresis followed by cutting the gels into their individual lanes that were incubated in 10 mM sodium acetate buffer (pH 5.5) in the absence (Nil) or presence of 10 μM E-64, ATV, or RTV. Gelatinolytic bands indicative of enzymatic activity were revealed by negative staining with amide black solution. Molecular mass markers are indicated.

ATV inhibits SARS-CoV-2 Mpro enzymatic activity. Next, we evaluated whether ATV could inhibit SARS-CoV-2 Mpro activity by partially purifying the enzyme in cellular fractions obtained from SARS-CoV-2-infected cells and performing zymographic profiles. To ensure that the proteinase profiles were not dependent on cellular enzymes, similar fractions of mock-infected cells were also prepared. The results from cysteine proteinase zymographic profiles in gelatinolytic gels revealed a cellular-related band of approximately 70 kDa under both conditions (Fig. 2, Nil lanes). This activity was blocked by the drug E-64, an epoxide that acts as an irreversible inhibitor of cysteine proteases (Fig. 2, E-64 lanes). In the infected cells, a region of activity was observed between 31 and 38 kDa that was not present in the mock fraction (Fig. 2). This zone of molecular weight is consistent with the expected size of SARS-CoV-2 Mpro. The enzyme activity was inhibited by exposure of the gels to 10 μM ATV, without affecting cellular cysteine proteinase (Fig. 2, ATV lanes). As a control, the activity of SARS-CoV-2 Mpro in fractions from infected cells was evaluated by treatment with RTV, which inhibited activity in the molecular range of 31 to 38 kDa without a change in the 70-kDa region (Fig. 2, RTV lanes). These data are consistent with predictions from the molecular modeling and dynamics that ATV targets SARS-CoV-2 Mpro.

SARS-CoV-2 is susceptible to ATV and ATV/RTV in different cell types. We extended our investigation to evaluate the susceptibility of SARS-CoV-2 to ATV in different cellular systems. Vero cells are a well-known model to produce high virus titers. ATV alone or in combination with RTV decreased infectious virus production and RNA levels in this cell line (Fig. 3A and B, respectively). ATV/RTV was more potent than ATV, with 50% effective concentration (EC_{50}) values of $0.5 \pm 0.08 \mu\text{M}$ and $2.0 \pm 0.12 \mu\text{M}$, respectively (Fig. 3B). Positive controls CQ, LPV/RTV, and remdesivir displayed potencies of $1.0 \pm 0.07 \mu\text{M}$, $5.3 \pm 0.5 \mu\text{M}$, and $0.5 \pm 0.08 \mu\text{M}$, respectively (Fig. 3B). Our positive controls are consistent with results in the literature (21), validating our analysis. The ATV/RTV, ATV, CQ, LPV/RTV, and remdesivir values for 50% cytotoxic concentration (CC_{50}) were $280 \pm 3 \mu\text{M}$, $312 \pm 8 \mu\text{M}$, $259 \pm 5 \mu\text{M}$, $91 \pm 3 \mu\text{M}$, and $512 \pm 30 \mu\text{M}$, respectively. Our results indicate that the selectivity index (SI; which represents the ratio between the CC_{50} and EC_{50} values) for ATV/RTV, ATV, CQ, LPV/RTV, and remdesivir were 560, 156, 259, 18, and 1,020, respectively, which shows that ATV/RTV and ATV have therapeutic potential above that of CQ and LPV/RTV, compounds that advanced toward clinical trials early after the pandemic outbreak.

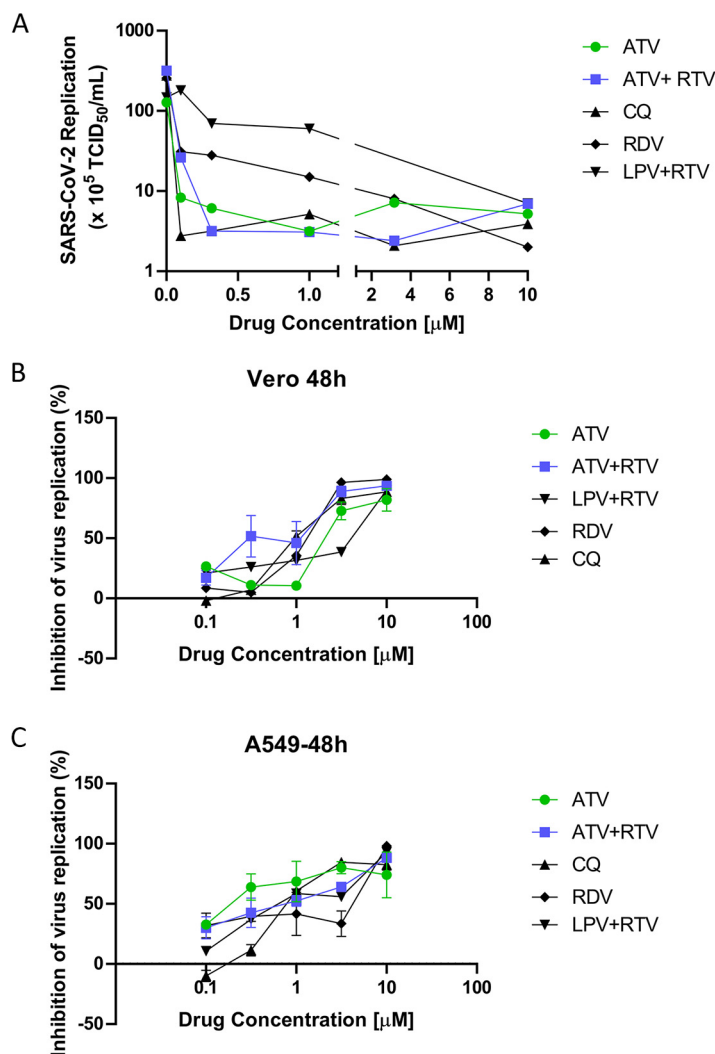


FIG 3 The antiviral activity of ATV and ATV/RTV against SARS-CoV-2. Vero (A and B) or A549 (C) cells were infected with SARS-CoV-2 at an MOI of 0.01 and exposed to the indicated concentrations of atazanavir (ATV), atazanavir/ritonavir (ATV/RTV; 3:1), chloroquine (CQ), remdesivir (RDV), or lopinavir/ritonavir (LPV/RTV; 4:1). After 2 days, viral replication in the culture supernatant was measured by TCID₅₀/ml (A) or RT-PCR (B and C). The data represent means \pm standard errors of the means (SEMs) from three independent experiments.

Since the results regarding the pharmacologic activity of ATV and ATV/RTV against SARS-CoV-2 replication in Vero cells were promising, we next investigated whether the proposed drug therapies could inhibit virus replication in a human epithelial pulmonary cell line (A549). ATV alone showed a nearly 10-fold increase in potency for inhibiting SARS-CoV-2 replication in A549 cells (Fig. 3C) compared to that in Vero cells (Fig. 3B). ATV/RTV and CQ were similarly potent in inhibiting virus replication in both cell types (Fig. 3B and C). Drugs repurposed in this study, ATV and ATV/RTV, were more potent than positive controls in inhibiting SARS-CoV-2 replication in A549 cells. Potencies for ATV/RTV, ATV, CQ, LPV/RTV, and remdesivir were $0.60 \pm 0.05 \mu\text{M}$, $0.22 \pm 0.02 \mu\text{M}$, $0.89 \pm 0.02 \mu\text{M}$, $0.9 \pm 0.5 \mu\text{M}$, and $0.6 \pm 0.02 \mu\text{M}$, respectively. *In vitro* results confirmed the rationale that SARS-CoV-2 would be susceptible to ATV, including in cells derived from the respiratory tract.

ATV and ATV/RTV prevent cell death and proinflammatory cytokine production in SARS-CoV-2-infected monocytes. Severe COVID-19 has been associated with levels of lactate dehydrogenase (LDH), interleukin 6 (IL-6), and leukopenia (22). Viral infection in the respiratory tract often triggers the migration of blood monocytes to

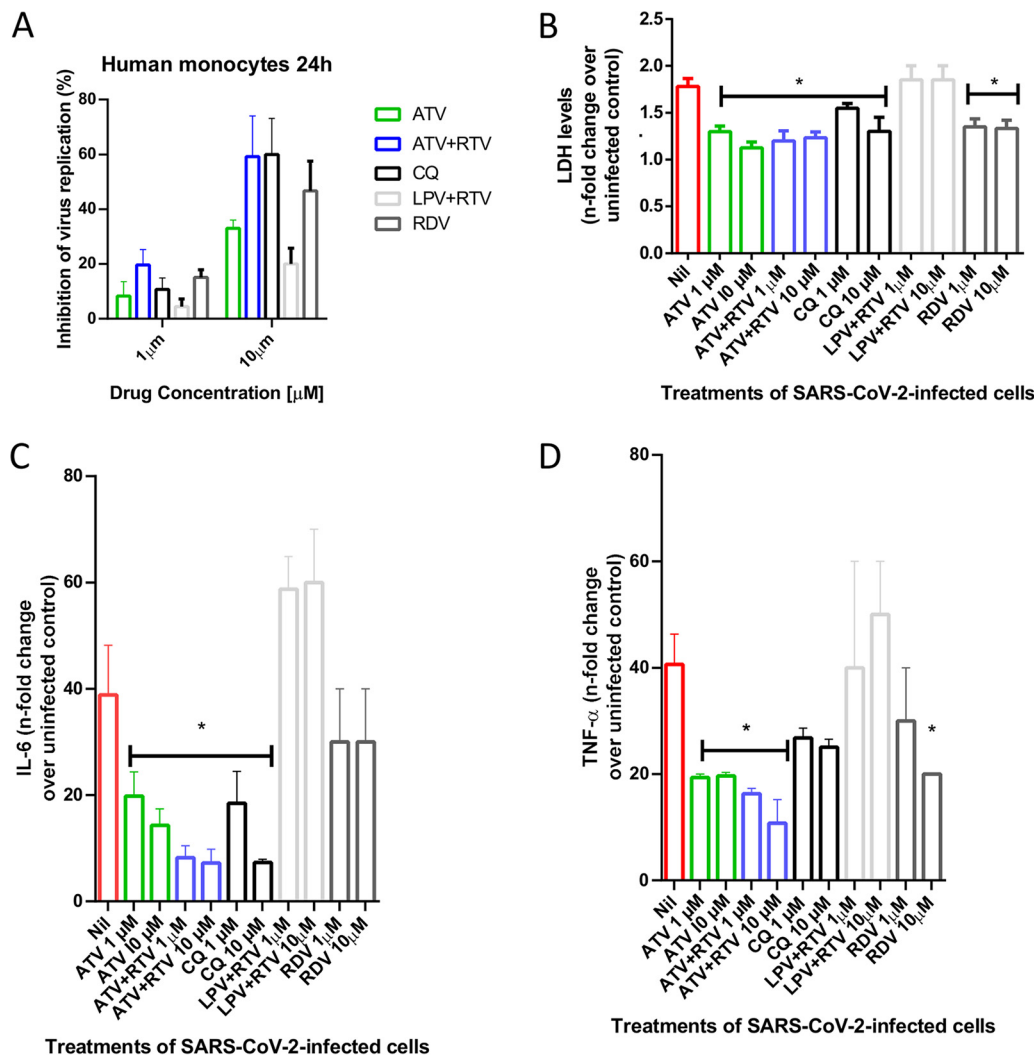


FIG 4 ATV and ATV/RTV impair SARS-CoV-2 replication, cell death, and cytokine storms in human primary monocytes. Human primary monocytes were infected at an MOI of 0.01 and treated with the indicated concentrations of atazanavir (ATV), atazanavir/ritonavir (ATV/RTV; 3:1), chloroquine (CQ), remdesivir (RDV), or lopinavir/ritonavir (LPV/RTV; 4:1). After 24 h, cell-associated subgenomic RNA levels (A) and LDH release (B) as well as the levels of IL-6 (C) and TNF- α (D) were measured in the culture supernatant. The data represent means \pm standard deviations (SDs) of experiments with cells from at least three healthy donors. *, $P < 0.05$ compared to untreated cells (Nil).

orchestrate the transition from innate to adaptive immune responses (23). For these reasons, ATV and ATV/RTV were tested at suboptimal (1 μ M) and optimal (10 μ M) doses, with respect to their *in vitro* pharmacological parameters against SARS-CoV-2.

ATV/RTV, CQ, and remdesivir were similarly efficient at reducing the amount viral genome equivalent in the human monocytes (Fig. 4A). Virus infection increased cellular mortality by 75%, which was prevented by ATV, ATV/RTV, and remdesivir (Fig. 4B). LPV/RTV was inefficient at reducing viral RNA levels and cell death (Fig. 4A and B). Moreover, we observed that infections by SARS-CoV-2 triggered the expected increase in the IL-6 levels in the culture supernatant, which ranged from 20- to 60-fold depending on the cell donor (Fig. 4C). The virus-induced enhancement of IL-6 levels was significantly prevented by treatment with ATV, ATV/RTV, and CQ (Fig. 4C). Another biomarker of uncontrolled proinflammatory cytokine response, tumor necrosis factor alpha (TNF- α), was upregulated 40-fold during virus infection (Fig. 4D). ATV, ATV/RTV, and remdesivir (10 μ M) significantly prevented the induction of TNF- α release (Fig. 4D). Altogether, our results confirm that ATV and ATV/RTV should not be ignored as an additional therapeutic option against COVID-19.

DISCUSSION

In these 2 decades of the 21st century, the human vulnerability to emerging viral diseases has been notable (24). The emergence of infectious disease highlights the undeniable fact that existing countermeasures are inefficient at preventing virus spill-over and disease outbreaks. Preclinical data on the susceptibility of an emerging virus to clinically approved drugs can allow for the rapid mobilization of resources toward clinical trials (8). This approach proved feasible for combating the Zika, yellow fever, and chikungunya outbreaks experienced in Brazil over the past 5 years, when our group demonstrated that sofosbuvir, a blockbuster drug against hepatitis C, could represent a compassionate countermeasure against these diseases (25–29).

Currently, the rate of SARS-CoV-2 dissemination has become one of the most rapidly evolving pandemics known in modern times, with the number of cases and deaths doubling every week, and the peak of the pandemic has yet to arrive in some territories (6). The existence of several ongoing clinical trials against COVID-19 reinforces the suggestion that drug repurposing represents the fastest approach to identify therapies to emerging infectious disease (8).

Among therapies initially included in the Solidarity trial, the most interesting results come from remdesivir, whereas CQ and LPV/RTV showed limited clinical benefit (9). LPV/RTV reduced mortality in critically ill patients by 5% (11). On the other hand, this therapy showed no clinical benefit in a large clinical trial (30). Although the combination therapy with protease (LPV/RTV) and RNA polymerase (ribavirin) inhibitors and immunomodulators (IFN- β) reduced the viral loads in COVID-19 patients (31), these drugs seem to be impractical for early treatment because of IFN's price-safety profile. The history of antiretroviral research teaches us that combinations are necessary. Positive laboratory and clinical results with RNA polymerase inhibitors, such as remdesivir, ribavirin, and favipiravir (21, 31, 32), against SARS-CoV-2 suggest they could be more effective if combined with active protease inhibitors. We highlight ATV and ATV/RTV because our assay readout to quantify infectious virus particles reveals (i) a good profile of antiviral activity, (ii) higher potencies in respiratory cells, and (iii) the ability to reduce levels of proinflammation mediator in monocytes.

We believe that early repurposing of LPV/RTV for COVID-19 was based on previous evidence during the SARS-CoV outbreak in 2002 and again for MERS-CoV (33). Information on the susceptibility of SARS-CoV-2 to other antiviral protease inhibitors approved since 2003, such as ATV, has been scarce. Since this year, ATV has become a wider prescribed drug among HIV-infected individuals than LPV, including for critically ill patients (17). ATV shows a safer profile than LPV in both short- and long-term therapeutic regimens (16, 34). ATV has a documented bioavailability to reach the respiratory tract (19, 35), which led to its proposed use against pulmonary fibrosis (20). Under our experimental conditions, ATV was superior to LPV/RTV, which may motivate further clinical trials.

The potency of LPV/RTV against SARS-CoV-2 was lower than those of ATV and ATV/RTV. Nevertheless, remdesivir was more potent than ATV or ATV/RTV. The improved potency of ATV, in comparison to that of LPV, may be at least in part due to its multiple hydrogen bond-driven interactions within the Mpro active site. Other investigators have also recognized a wider range of interactions of ATV and Mpro compared to those with LPV (18, 36), although none provided functional evidence through phenotypic assays as presented here. Neither ATV nor LPV displayed any interactions with the catalytic dyad of Cys145 and His41 at the start of the molecular dynamics simulations. However, important interactions were observed at the end, such as LPV-His41 and ATV-Glu166. Glu166 is one of the residues that promotes the opening of Mpro for its substrate to interact with the active site (37, 38).

Highly pathogenic respiratory viruses, such as influenza A virus, have been associated with a cytokine storm, described as an uncontrolled proinflammatory cytokine response (39, 40). Cytokine storms also seem to be highly relevant for pathogenic human CoVs (41). Contemporary investigations on SARS-CoV-2 strongly suggest the

involvement of cytokine storms in disease severity (22). COVID-19 mortality is associated with enhanced IL-6 levels and consistent with cell death, as measured by LDH release (22). We showed that ATV and ATV/RTV decreased IL-6 release in SARS-CoV-2-infected human primary monocytes. Moreover, we also included in our analysis TNF- α , another hallmark of inflammation during respiratory virus infections (22, 58). Our results revealed that cellular mortality and cytokine storm-associated mediators were reduced after treatment with the repurposed antiretroviral drugs used in this study.

As the SARS-CoV-2 pandemic goes on and the Solidarity trials fail to demonstrate the benefit of LPV/RTV, preclinical data or clinically approved protease inhibitors, such as ATV-ATV/RTV, need to be catalogued. The higher potency of ATV-ATV/RTV over that of LPV/RTV is the contribution of our study to highlight a new option among clinically approved drugs that should be considered in ongoing clinical trials for an effective treatment for COVID-19.

MATERIALS AND METHODS

Reagents. The antivirals ATV, ATV/RTV, and CQ were received as donations from Instituto de Tecnologia de Fármacos (Farmanguinhos, Fiocruz). ATV/RTV was prepared daily in the proportion of 3:1 as pharmaceutical pills composed of 300 mg ATV and 100 mg RTV. Remdesivir and LPV/RTV (4:1 ratio) were purchased from Selleckchem (Houston, TX). Enzyme-linked immunosorbent assay (ELISA) kits were purchased from R&D Bioscience. All small molecule inhibitors were dissolved in 100% dimethyl sulfoxide (DMSO) and subsequently diluted at least 10^4 -fold in culture or reaction medium before each assay. The final DMSO concentrations showed no cytotoxicity. The materials for cell culture were purchased from Thermo Scientific Life Sciences (Grand Island, NY), unless otherwise mentioned.

Triton X-100 (TX-100), 3-[[3-(cholamidopropyl)-dimethylammonio]-1-propanesulfonate hydrate (CHAPS), 1,2,3-propanetriol (glycerol), bovine serum albumin (BSA), phosphate-buffered saline (PBS), *N*-benzyloxy-carbonyl-L-phenylalanyl-L-arginine 7-amino-4-methylcoumarin (Z-FR-AMC; $\epsilon = 1.78 \times 10^4 \text{ M}^{-1} \text{ cm}^{-1}$), dithiothreitol (DTT), and *trans*-epoxysuccinyl-L-leucylamido(4-guanidino)butane (E-64) were purchased from Sigma-Aldrich Chemical Co. (St. Louis, MO, USA). HiTrap Q FF anion-exchange chromatography columns (HiTrap Q FF) were purchased from GE Healthcare Life Sciences. A Micro bicinchoninic acid (BCA) protein assay kit was purchased from Pierce Chemical Co. (Appleton, WI). All other reagents were of analytical grade or better.

Cells and virus. African green monkey kidney (Vero, subtype E6) and A549 (human lung epithelial cells) cells were cultured in high-glucose Dulbecco's modified Eagle medium (DMEM) with 10% fetal bovine serum (FBS; HyClone, Logan, UT) and 100 U/ml penicillin and 100 $\mu\text{g/ml}$ streptomycin (pen/strep; Thermo Fisher) at 37°C in a humidified atmosphere with 5% CO₂.

Human primary monocytes were obtained after 3 h of plastic adherence of peripheral blood mononuclear cells (PBMCs). PBMCs were isolated from healthy donors by density gradient centrifugation (Ficoll-Paque; GE Healthcare). PBMCs (2.0×10^6 cells) were plated on 48-well plates (Nalge Nunc) in RPMI 1640 without serum for 2 to 4 h. Nonadherent cells were removed, and the remaining monocytes were maintained in DMEM with 5% human serum (HS; Millipore) and penicillin/streptomycin. The purity of human monocytes was >95% as determined by flow cytometric analysis (FACScan; Becton, Dickinson) using anti-CD3 (BD Biosciences) and anti-CD16 (Southern Biotech) monoclonal antibodies.

SARS-CoV-2 was prepared in Vero E6 cells from an isolate contained on a nasopharyngeal swab obtained from a confirmed case in Rio de Janeiro, Brazil. Viral experiments were performed after a single passage in a cell culture in a 150-cm² flask with DMEM plus 2% FBS. Observations for cytopathic effects were performed daily, which peaked 4 to 5 days after infection. All procedures related to virus culture were handled in a biosafety level 3 (BSL3) multiuser facility according to WHO guidelines. Virus titers were determined as the tissue culture infectious dose at 50% (TCID₅₀/ml). Virus stocks were kept in -80°C ultralow freezers. The virus strain was sequenced to confirm the virus identity.

Cytotoxicity assay. Monolayers of 1.5×10^4 Vero cells in 96-well plates were treated for 3 days with various concentrations (semilog dilutions from 600 to 10 μM) of ATV, ATV/RTV, or CQ. Then, 5 mg/ml 2,3-bis-(2-methoxy-4-nitro-5-sulfo-phenyl)-2*H*-tetrazolium-5-carboxanilide (XTT) in DMEM was added to the cells in the presence of 0.01% of *N*-methyl dibenzopyrazine methyl sulfate (PMS). After incubating for 4 h at 37°C, the plates were measured in a spectrophotometer at 492 nm and 620 nm. The 50% cytotoxic concentration (CC₅₀) was calculated by a nonlinear regression analysis of the dose-response curves.

Yield reduction assay. Cells were infected at a multiplicity of infection (MOI) of 0.01. Vero or A549 cells were infected at densities of 5×10^5 cells/well. Human primary monocytes were infected at a density of 2×10^5 to 8×10^5 cells/well, depending on the endogenous characteristic of the cell donor. Infections were performed in 48-well plates for 2 h at 37°C. The cells were washed, and various concentrations of compounds were added to DMEM with 2% FBS. After 48 h, virus in the supernatants was quantified by real-time reverse transcription-PCR (RT-PCR) and/or by TCID₅₀/ml. A variable slope nonlinear regression analysis of the dose-response curves was performed to calculate the concentration at which each drug inhibited virus production by 50% (EC₅₀).

Virus titration. Monolayers of Vero cells (2×10^4 cell/well) in 96-well plates were infected with a log-based dilution of supernatants containing SARS-CoV-2 for 1 h at 37°C. Cells were washed, fresh medium was added with 2% FBS, and 3 to 5 days postinfection, the cytopathic effect was scored in at

least 10 replicates per dilution by independent readers. The reader was blind with respect to source of the supernatant. A Reed and Muench scoring method was employed to determine TCID₅₀/ml (42).

Molecular detection of virus RNA levels. The total RNA from the culture supernatants was extracted using a QIAamp Viral RNA kit (Qiagen), according to the manufacturer's instructions. Quantitative RT-PCR was performed using a QuantiTect Probe RT-PCR kit (Qiagen) in an ABI PRISM 7500 sequence detection system (Applied Biosystems). Amplifications were carried out in 25- μ l reaction mixtures containing 2 \times reaction mix buffer, 50 μ M each primer, 10 μ M probe, and 5 μ l of RNA template. Primers, probes, and cycling conditions recommended by the Centers for Disease Control and Prevention (CDC) protocol were used to detect SARS-CoV-2 (43). The standard curve method was employed for virus quantification. For reference to the cell amounts used, the housekeeping gene RNase P was amplified. The threshold cycle (C_T) values for this target were compared to those obtained for different cell amounts, 10⁷ to 10², for calibration.

Measurements of inflammatory mediators and cell death marker. The levels of TNF- α , IL-6, and LDH were quantified in the monocyte supernatants from infected and uninfected cells. ELISAs for TNF- α and IL-6 required 100 μ l of supernatants to be exposed to capture antibody in 96-well plates. After a 2-h incubation period at room temperature (RT), the detection antibody was added. Plates were incubated for another 2 h at RT. Streptavidin-horseradish peroxidase (HRP) and its substrate were added and incubated for 20 min, and the optical density was determined using a microplate reader set to 450 nm.

Extracellular lactate dehydrogenase (LDH) was quantified using a Duo kit according to the manufacturer's instructions. Supernatant was centrifuged at 5,000 rpm for 1 min to remove cellular debris. A total of 25 μ l of supernatant was placed into 96-well plates and incubated with 5 μ l of ferric alum and 100 μ l of LDH substrate for 3 min at 37°C. NAD (oxidized form) was added before the addition of a stabilizing solution. After a 10-min incubation, plates were measured in a spectrophotometer at 492 nm.

Molecular docking. ATV (PubChem CID 148192) and LPV (PubChem CID 92727) were used as inhibitors of the SARS-CoV-2 Mpro. ATV and LPV were prepared using a generalized amber force field (GAFF), and their charges were obtained using the AM1-BCC loading scheme (44, 45).

Molecular docking experiments were performed with DOCK 6.9 (46) to identify the binding site of Mpro. SARS-CoV-2 Mpro structure was obtained from Protein Data Bank (RCSB PDB; <http://www.rcsb.org>) under the accession code 6LU7 (47). The active site region was identified by using a complexed peptide {N-[(5-methylisoxazol-3-yl)carbonyl]alanyl-L-valyl-L-1-[[1R,2Z]-4-(benzyloxy)-4-oxo-1-[(3R)-2-oxopyrrolidin-3-yl]methyl]-2-enyl]-L-leucinamide} as a guide. The creation of the DOCK 6.9 input files for docking was performed using Chimera 1.14 (48).

The docking of ligands was performed in a box of 10-Å edges with its mass center matching that of the complexed peptide. Each scan produced 20 conformations for each ligand, with the best score being used for molecular dynamics simulations.

Molecular dynamics. Since the tertiary structure (3D) of the SARS-CoV-2 Mpro is a homodimer, we focused the molecular dynamics on only one chain, chain A. Molecular dynamics calculations were performed using NAMD 2.9 (49) and Charmm27* force field (50) at pH 7, i.e., with deprotonated Glu and Asp, protonated Arg and Lys, and neutral His with a protonated N ϵ atom. This all-atom force field has been able to fold properly many soluble proteins (51–53). The soluble proteins were centered in a cubic box of transferable intermolecular potential with 3 points (TIP3P) water molecules (54); the box extended 1.2 nm outside the protein on its four lateral sides, and the appropriate numbers of Na⁺ and Cl⁻ ions were added to ensure system neutralization. The electrostatic interactions were calculated using the particle mesh Ewald method and a cutoff of 1.2 nm (55). The same cutoff of 1.2 nm was used for the Van der Waals interactions. The nonbonded pair lists were updated every 10 fs. The analysis was based on molecular dynamics (MD) simulation of 100 ns at 310 K.

Protein extraction. Protein extracts containing SARS-CoV-2 Mpro activity were obtained from Vero cell monolayers on 25-cm² flasks that were infected for 1 h at an MOI of 0.1 at 37°C and 5% CO₂. After 1 or 2 days of infection, the supernatant was harvested, and monolayers were washed 3 times with in sterile cold PBS (pH 7.2). Next, cells were suspended in 1 ml of lysis buffer (100 mM Tris-HCl [pH 8.0], 150 mM NaCl, 10% glycerol, and 0.6% Triton X-100) and kept at 4°C. The soluble protein fraction was isolated as the supernatant after centrifugation (100,000 \times g, 30 min, 4°C) and stored at -20°C until further use. The protein concentrations of the samples were determined using the BCA protein assay kit.

Zymographic assays. Proteinases were assayed after electrophoresis on 10% SDS-PAGE gels with 0.1% copolymerized gelatin (56). Briefly, each of the gel slots was loaded with 12 μ g of soluble proteins dissolved in Laemmli's buffer, and following electrophoresis at a constant voltage of 200 V at 4°C, they were soaked for 1 h at 25°C in washing buffer (0.1 mM sodium acetate buffer [pH 5.5] containing 2.5% TX-100). Proteinase activity was detected by incubating (16 h at 37°C) the gels in reaction buffer (0.1 mM sodium acetate buffer pH 5.5 containing 1.0 mM DTT), in the presence or absence of the same concentrations of 10 μ M E-64, ATV, RTV, or the ATV/RTV combination. Hydrolysis of gelatin was visualized by staining the gels with 0.2% amido black (57).

Statistical analysis. The assays were performed blinded by one professional, codified, and then read by another professional. All experiments were carried out at least three independent times, including a minimum of two technical replicates in each assay. The dose-response curves used to calculate EC₅₀ and CC₅₀ values were generated by variable slope plot from Prism GraphPad software 8.0. The equations to fit the best curve were generated based on R² values of \geq 0.9. Student's *t* test was used to assess statistical significance at *P* values of <0.05. The statistical analyses specific to each software program used in the bioinformatics analysis are described above.

Data availability. The complete genome of the virus strain used in this study is publicly available at <https://nextstrain.org/ncov> (Brazil/RJ-314/2020 or GISAID EPI_ISL no. 414045).

SUPPLEMENTAL MATERIAL

Supplemental material is available online only.

SUPPLEMENTAL FILE 1, PDF file, 1.2 MB.

ACKNOWLEDGMENTS

We thank Carmen Beatriz Wagner Giacoia Gripp for assessments related to the BSL3 facility.

This work was supported by Conselho Nacional de Desenvolvimento Científico e Tecnológico (CNPq), Fundação de Amparo à Pesquisa do Estado do Rio de Janeiro (FAPERJ). This study was financed in part by the Coordenação de Aperfeiçoamento de Pessoal de Nível Superior—Brasil (CAPES), finance code 001. Funding was also provided by CNPq, CAPES, and FAPERJ through the National Institutes of Science and Technology Program (INCT) to Carlos Morel (INCT-IDPN). Support was also provided by the Oswaldo Cruz Foundation/Fiocruz under the auspices of the Inova program. The funding sponsors had no role in the design of the study, in the collection, analyses, or interpretation of data, in the writing of the manuscript, and in the decision to publish the results.

Experimental execution and analysis—N.F.-R., C.Q.S., C.R.L., F.S.D.S., A.C.F., M.M., C.S.D.F., V.C.S., S.S.S.G.D., J.R.T., M.D.M., and A.R.M.; data analysis, manuscript preparation and revision—N.F.-R., C.Q.S., A.C.F., C.S.D.F., C.R.L., F.S.D.S., F.A.B., N.C., C.R.A., M.M.S., P.T.B., and T.M.L.S.; conceptualized the experiments—N.F.-R., C.Q.S., and T.M.L.S.; study coordination—T.M.L.S.; manuscript preparation and revision—P.T.B. and T.M.L.S.

We declare no competing financial interests.

REFERENCES

- Masters PS. 2006. The molecular biology of coronaviruses. *Adv Virus Res* 66:193–292. [https://doi.org/10.1016/S0065-3527\(06\)66005-3](https://doi.org/10.1016/S0065-3527(06)66005-3).
- Cui J, Li F, Shi Z-L. 2019. Origin and evolution of pathogenic coronaviruses. *Nat Rev Microbiol* 17:181–192. <https://doi.org/10.1038/s41579-018-0118-9>.
- Lam TT-Y, Jia N, Zhang Y-W, Shum MH-H, Jiang J-F, Zhu H-C, Tong Y-G, Shi Y-X, Ni X-B, Liao Y-S, Li W-J, Jiang B-G, Wei W, Yuan T-T, Zheng K, Cui X-M, Li J, Pei G-Q, Qiang X, Cheung WY-M, Li L-F, Sun F-F, Qin S, Huang J-C, Leung GM, Holmes EC, Hu Y-L, Guan Y, Cao W-C. 2020. Identifying SARS-CoV-2 related coronaviruses in Malayan pangolins. *Nature* 583:282–285. <https://doi.org/10.1038/s41586-020-2169-0>.
- World Health Organization. 2020. Middle east respiratory syndrome coronavirus (MERS-CoV). <https://www.who.int/emergencies/mers-cov/en/>. Accessed 24 July 2020.
- World Health Organization. 2020. Severe acute respiratory syndrome (SARS). <https://www.who.int/health-topics/severe-acute-respiratory-syndrome>. Accessed 24 July 2020.
- Dong E, Du H, Gardner L. 2020. An interactive web-based dashboard to track COVID-19 in real time. *Lancet Infect Dis* 20:533–534. [https://doi.org/10.1016/S1473-3099\(20\)30120-1](https://doi.org/10.1016/S1473-3099(20)30120-1).
- Romer P, Garber AM. 2020. Opinion. Will our economy die from coronavirus? *The New York Times*. <https://www.nytimes.com/2020/03/23/opinion/coronavirus-depression.html>. Accessed 24 July 2020.
- Harrison C. 2020. Coronavirus puts drug repurposing on the fast track. *Nat Biotechnol* 38:379–381. <https://doi.org/10.1038/d41587-020-00003-1>.
- World Health Organization. 2020. WHO R&D Blueprint: informal consultation on prioritization of candidate therapeutic agents for use in novel coronavirus 2019 infection, Geneva, Switzerland, WHO/HEO/R&D Blueprint (nCoV)/2020.1. <https://apps.who.int/iris/handle/10665/330680>. Accessed 24 July 2020.
- Borba MGS, Val FFA, Sampaio VS, Alexandre MAA, Melo GC, Brito M, Mourão MPG, Brito-Sousa JD, Baía-da-Silva D, Guerra MVF, Hajjar LA, Pinto RC, Balieiro AAS, Pacheco AGF, Santos JDO, Naveca FG, Xavier MS, Siqueira AM, Schwarzbald A, Croda J, Nogueira ML, Romero GAS, Bassat Q, Fontes CJ, Albuquerque BC, Daniel-Ribeiro C-T, Monteiro WM, Lacerda MVG, CloroCovid-19 Team. 2020. Effect of high vs low doses of chloroquine diphosphate as adjunctive therapy for patients hospitalized with severe acute respiratory syndrome coronavirus 2 (SARS-CoV-2) infection: a randomized clinical trial. *JAMA Netw Open* 3:e208857. <https://doi.org/10.1001/jamanetworkopen.2020.8857>.
- Cao B, Wang Y, Wen D, Liu W, Wang J, Fan G, Ruan L, Song B, Cai Y, Wei M, Li X, Xia J, Chen N, Xiang J, Yu T, Bai T, Xie X, Zhang L, Li C, Yuan Y, Chen H, Li H, Huang H, Tu S, Gong F, Liu Y, Wei Y, Dong C, Zhou F, Gu X, Xu J, Liu Z, Zhang Y, Li H, Shang L, Wang K, Li K, Zhou X, Dong X, Qu Z, Lu S, Hu X, Ruan S, Luo S, Wu J, Peng L, Cheng F, Pan L, Zou J, Jia C, Wang J, Liu X, Wang S, Wu X, Ge Q, He J, Zhan H, Qiu F, Guo L, Huang C, Jaki T, Hayden FG, Horby PW, Zhang D, Wang C. 2020. A trial of lopinavir-ritonavir in adults hospitalized with severe COVID-19. *N Engl J Med* 382:1787–1799. <https://doi.org/10.1056/NEJMoa2001282>.
- De Clercq E, Li G. 2016. Approved Antiviral drugs over the past 50 years. *Clin Microbiol Rev* 29:695–747. <https://doi.org/10.1128/CMR.00102-15>.
- Wu C-Y, Jan J-T, Ma S-H, Kuo C-J, Juan H-F, Cheng Y-SE, Hsu H-H, Huang H-C, Wu D, Brik A, Liang F-S, Liu R-S, Fang J-M, Chen S-T, Liang P-H, Wong C-H. 2004. Small molecules targeting severe acute respiratory syndrome human coronavirus. *Proc Natl Acad Sci U S A* 101:10012–10017. <https://doi.org/10.1073/pnas.0403596101>.
- Fehr AR, Perlman S. 2015. Coronaviruses: an overview of their replication and pathogenesis. *Methods Mol Biol* 1282:1–23. https://doi.org/10.1007/978-1-4939-2438-7_1.
- Gong Y, Haque S, Chowdhury P, Cory TJ, Kodidela S, Yallapu MM, Norwood JM, Kumar S. 2019. Pharmacokinetics and pharmacodynamics of cytochrome P450 inhibitors for HIV treatment. *Expert Opin Drug Metab Toxicol* 15:417–427. <https://doi.org/10.1080/17425255.2019.1604685>.
- Stanley TL, Joy T, Hadigan CM, Liebau JG, Makimura H, Chen CY, Thomas BJ, Weise SB, Robbins GK, Grinspoon SK. 2009. Effects of switching from lopinavir/ritonavir to atazanavir/ritonavir on muscle glucose uptake and visceral fat in HIV-infected patients. *AIDS* 23:1349–1357. <https://doi.org/10.1097/QAD.0b013e32832ba904>.
- Gibert CL. 2016. Treatment guidelines for the use of antiretroviral agents in HIV-infected adults and adolescents: an update. *Fed Pract* 33:315–365.
- Dayer MR. 2020. Old drugs for newly emerging viral disease, COVID-19: bioinformatic prospective. *arXiv* 2003.04524 [q-bio.BM] <https://arxiv.org/abs/2003.04524>.
- Gautam N, Roy U, Balkundi S, Puligujja P, Guo D, Smith N, Liu X-M, Lamberty B, Morse B, Fox HS, McMillan J, Gendelman HE, Alnouti Y. 2013. Preclinical pharmacokinetics and tissue distribution of long-acting nanoformulated antiretroviral therapy. *Antimicrob Agents Chemother* 57:3110–3120. <https://doi.org/10.1128/AAC.00267-13>.
- Song S, Ji Y, Zhang G, Zhang X, Li B, Li D, Jiang W. 2018. Protective effect of atazanavir sulphate against pulmonary fibrosis *in vivo* and *in vitro*. *Basic Clin Pharmacol Toxicol* 122:199–207. <https://doi.org/10.1111/bcpt.12871>.

21. Wang M, Cao R, Zhang L, Yang X, Liu J, Xu M, Shi Z, Hu Z, Zhong W, Xiao G. 2020. Remdesivir and chloroquine effectively inhibit the recently emerged novel coronavirus (2019-nCoV) *in vitro*. *Cell Res* 30:269–271. <https://doi.org/10.1038/s41422-020-0282-0>.
22. Zhou F, Yu T, Du R, Fan G, Liu Y, Liu Z, Xiang J, Wang Y, Song B, Gu X, Guan L, Wei Y, Li H, Wu X, Xu J, Tu S, Zhang Y, Chen H, Cao B. 2020. Clinical course and risk factors for mortality of adult inpatients with COVID-19 in Wuhan, China: a retrospective cohort study. *Lancet* 395: 1054–1062. [https://doi.org/10.1016/S0140-6736\(20\)30566-3](https://doi.org/10.1016/S0140-6736(20)30566-3).
23. Newton AH, Cardani A, Braciale TJ. 2016. The host immune response in respiratory virus infection: balancing virus clearance and immunopathology. *Semin Immunopathol* 38:471–482. <https://doi.org/10.1007/s00281-016-0558-0>.
24. Solomon T, Baylis M, Brown D. 2016. Zika virus and neurological disease—approaches to the unknown. *Lancet Infect Dis* 16:402–404. [https://doi.org/10.1016/S1473-3099\(16\)00125-0](https://doi.org/10.1016/S1473-3099(16)00125-0).
25. de Freitas CS, Higa LM, Sacramento CQ, Ferreira AC, Reis PA, Delvecchio R, Monteiro FL, Barbosa-Lima G, James Westgarth H, Vieira YR, Mattos M, Rocha N, Hoelz LVB, Leme RPP, Bastos MM, L Rodrigues GO, M Lopes CE, Queiroz-Junior CM, Lima CX, Costa VV, Teixeira MM, Bozza FA, Bozza PT, Boechat N, Tanuri A, Souza TML. 2019. Yellow fever virus is susceptible to sofosbuvir both *in vitro* and *in vivo*. *PLoS Negl Trop Dis* 13:e0007072. <https://doi.org/10.1371/journal.pntd.0007072>.
26. Ferreira AC, Reis PA, de Freitas CS, Sacramento CQ, Villas Bôas Hoelz L, Bastos MM, Mattos M, Rocha N, Gomes de Azevedo Quintanilha I, da Silva Gouveia Pedrosa C, Rocha Quintino Souza L, Correia Loiola E, Trindade P, Rangel Vieira Y, Barbosa-Lima G, de Castro Faria Neto HC, Boechat N, Rehen SK, Brüning K, Bozza FA, Bozza PT, Souza TML. 2018. Beyond members of the Flaviviridae family, sofosbuvir also inhibits chikungunya virus replication. *Antimicrob Agents Chemother* 63:e01389-18. <https://doi.org/10.1128/AAC.01389-18>.
27. Ferreira AC, Zaverucha-do-Valle C, Reis PA, Barbosa-Lima G, Vieira YR, Mattos M, de Paiva Silva P, Sacramento C, de Castro Fariaeto HC, Campanati L, Tanuri A, Brüning K, Bozza FA, Bozza PT, Souza TML. 2017. Sofosbuvir protects Zika virus-infected mice from mortality, preventing short- and long-term sequelae. *Sci Rep* 7:9409. <https://doi.org/10.1038/s41598-017-09797-8>.
28. Sacramento CQ, de Melo GR, de Freitas CS, Rocha N, Hoelz LV, Miranda M, Fintelman-Rodrigues N, Marttorelli A, Ferreira AC, Barbosa-Lima G, Abrantes JL, Vieira YR, Bastos MM, de Mello Volotão E, Nunes EP, Tschoeke DA, Leomil L, Loiola EC, Trindade P, Rehen SK, Bozza FA, Bozza PT, Boechat N, Thompson FL, de Filippis AM, Brüning K, Souza TM. 2017. The clinically approved antiviral drug sofosbuvir inhibits Zika virus replication. *Sci Rep* 7:40920. <https://doi.org/10.1038/srep40920>.
29. Figueiredo-Mello C, Casadio LVB, Avelino-Silva VI, Yeh-Li H, Sztajnbock J, Joelsons D, Antonio MB, Pinho JRR, de Mello Malta F, Gomes-Gouvêa MS, Salles APM, Corá AP, Moreira CHV, Ribeiro AF, de Seixas Santos Natri S, Malaque CMS, Teixeira RFA, Borges LMS, Gonzalez MP, Junior LCP, Souza TNL, Song ATW, D'Albuquerque LAC, Abdala E, Andraus W, de Martino RB, Ducatti L, Andrade GM, Malbouisson LMS, de Souza IM, Carrilho FJ, Sabino EC, Levin AS. 2019. Efficacy of sofosbuvir as treatment for yellow fever: protocol for a randomised controlled trial in Brazil (SOFFA study). *BMJ Open* 9:e027207. <https://doi.org/10.1136/bmjopen-2018-027207>.
30. Chief Investigators of the Randomised Evaluation of COVID-19 thERapY (RECOVERY) trial on lopinavir-ritonavir. 2020. No clinical benefit from use of lopinavir-ritonavir in hospitalised COVID-19 patients studied in RECOVERY. <https://www.recoverytrial.net/news/no-clinical-benefit-from-use-of-lopinavir-ritonavir-in-hospitalised-covid-19-patients-studied-in-recovery>. Accessed 24 July 2020.
31. Hung IF-N, Lung K-C, Tso EY-K, Liu R, Chung TW-H, Chu M-Y, Ng Y-Y, Lo J, Chan J, Tam AR, Shum H-P, Chan Y, Wu AK-L, Sin K-M, Leung W-S, Law W-L, Lung DC, Sin S, Yeung P, Yip CC-Y, Zhang RR, Fung AY-F, Yan EY-W, Leung K-H, Ip JD, Chu AW-H, Chan W-M, Ng AC-K, Lee R, Fung K, Yeung A, Wu T-C, Chan JW-M, Yan W-W, Chan W-M, Chan JF-W, Lie AK-W, Tsang OT-Y, Cheng VC-C, Que T-L, Lau C-S, Chan K-H, To KK-W, Yuen K-Y. 2020. Triple combination of interferon beta-1b, lopinavir-ritonavir, and ribavirin in the treatment of patients admitted to hospital with COVID-19: an open-label, randomised, phase 2 trial. *Lancet* 395:1695–1704. [https://doi.org/10.1016/S0140-6736\(20\)31042-4](https://doi.org/10.1016/S0140-6736(20)31042-4).
32. Cai Q, Yang M, Liu D, Chen J, Shu D, Xia J, Liao X, Gu Y, Cai Q, Yang Y, Shen C, Li X, Peng L, Huang D, Zhang J, Zhang S, Wang F, Liu J, Chen L, Chen S, Wang Z, Zhang Z, Cao R, Zhong W, Liu Y, Liu L. 2020. Experimental treatment with favipiravir for COVID-19: an open-label control study. *Engineering* <https://doi.org/10.1016/j.eng.2020.03.007>.
33. Sheahan TP, Sims AC, Leist SR, Schäfer A, Won J, Brown AJ, Montgomery SA, Hogg A, Babusis D, Clarke MO, Spahn JE, Bauer L, Sellers S, Porter D, Feng JY, Cihlar T, Jordan R, Denison MR, Baric RS. 2020. Comparative therapeutic efficacy of remdesivir and combination lopinavir, ritonavir, and interferon beta against MERS-CoV. 1. *Nat Commun* 11:1–14. <https://doi.org/10.1038/s41467-019-13940-6>.
34. Lv Z, Chu Y, Wang Y. 2015. HIV protease inhibitors: a review of molecular selectivity and toxicity. *HIV/AIDS (Auckl)* 7:95–104. <https://doi.org/10.2147/HIV.S79956>.
35. Huang J, Gautam N, Bathena SPR, Roy U, McMillan J, Gendelman HE, Alnouti Y. 2011. UPLC-MS/MS quantification of nanoformulated ritonavir, indinavir, atazanavir, and efavirenz in mouse serum and tissues. *J Chromatogr B Analyt Technol Biomed Life Sci* 879:2332–2338. <https://doi.org/10.1016/j.jchromb.2011.06.032>.
36. Beck BR, Shin B, Choi Y, Park S, Kang K. 2020. Predicting commercially available antiviral drugs that may act on the novel coronavirus (SARS-CoV-2) through a drug-target interaction deep learning model. *Comput Struct Biotechnol J* 18:784–790. <https://doi.org/10.1016/j.csbj.2020.03.025>.
37. Yang H, Yang M, Ding Y, Liu Y, Lou Z, Zhou Z, Sun L, Mo L, Ye S, Pang H, Gao GF, Anand K, Bartlam M, Hilgenfeld R, Rao Z. 2003. The crystal structures of severe acute respiratory syndrome virus main protease and its complex with an inhibitor. *Proc Natl Acad Sci U S A* 100:13190–13195. <https://doi.org/10.1073/pnas.1835675100>.
38. Macchiagodena M, Pagliai M, Procacci P. 2020. Identification of potential binders of the main protease 3CL^{pro} of the COVID-19 via structure-based ligand design and molecular modeling. *Chem Phys Lett* 750:137489. <https://doi.org/10.1016/j.cplett.2020.137489>.
39. Gao R, Bhatnagar J, Blau DM, Greer P, Rollin DC, Denison AM, DeLeon-Carnes M, Shieh WJ, Sambhara S, Tumpey TM, Patel M, Liu L, Paddock C, Drew C, Shu Y, Katz JM, Zaki SR. 2013. Cytokine and chemokine profiles in lung tissues from fatal cases of 2009 pandemic influenza A (H1N1): role of the host immune response in pathogenesis. *Am J Pathol* 183: 1258–1268. <https://doi.org/10.1016/j.ajpath.2013.06.023>.
40. Peschke T, Bender A, Nain M, Gerns D. 1993. Role of macrophage cytokines in influenza A virus infections. *Immunobiology* 189:340–355. [https://doi.org/10.1016/s0171-2985\(11\)80365-7](https://doi.org/10.1016/s0171-2985(11)80365-7).
41. Channappanavar R, Perlman S. 2017. Pathogenic human coronavirus infections: causes and consequences of cytokine storm and immunopathology. *Semin Immunopathol* 39:529–539. <https://doi.org/10.1007/s00281-017-0629-x>.
42. Reed LJ, Muench H. 1938. A simple method of estimating fifty percent endpoints. *Am J Hyg* 27:493–497.
43. CDC. 2020. Coronavirus disease 2019 (COVID-19). CDC, Atlanta, GA.
44. Jakalian A, Jack DB, Bayly CI. 2002. Fast, efficient generation of high-quality atomic charges. AM1-BCC model: II. Parameterization and validation. *J Comput Chem* 23:1623–1641. <https://doi.org/10.1002/jcc.10128>.
45. Wang J, Wolf RM, Caldwell JW, Kollman PA, Case DA. 2004. Development and testing of a general amber force field. *J Comput Chem* 25: 1157–1174. <https://doi.org/10.1002/jcc.20035>.
46. Allen WJ, Balius TE, Mukherjee S, Brozell SR, Moustakas DT, Lang PT, Case DA, Kuntz ID, Rizzo RC. 2015. DOCK 6: impact of new features and current docking performance. *J Comput Chem* 36:1132–1156. <https://doi.org/10.1002/jcc.23905>.
47. Jin Z, Du X, Xu Y, Deng Y, Liu M, Zhao Y, Zhang B, Li X, Zhang L, Duan Y, Yu J, Wang L, Yang K, Liu F, You T, Liu X, Yang X, Bai F, Liu H, Liu X, Guddat LW, Xiao G, Qin C, Shi Z, Jiang H, Rao Z, Yang H. 2020. Structure of M^{pro} from SARS-CoV-2 and discovery of its inhibitors. *Nature* 582: 289–293. <https://doi.org/10.1038/s41586-020-2223-y>.
48. Pettersen EF, Goddard TD, Huang CC, Couch GS, Greenblatt DM, Meng EC, Ferrin TE. 2004. UCSF Chimera—a visualization system for exploratory research and analysis. *J Comput Chem* 25:1605–1612. <https://doi.org/10.1002/jcc.20084>.
49. Phillips JC, Braun R, Wang W, Gumbart J, Tajkhorshid E, Villa E, Chipot C, Skeel RD, Kalé L, Schulten K. 2005. Scalable molecular dynamics with NAMD. *J Comput Chem* 26:1781–1802. <https://doi.org/10.1002/jcc.20289>.
50. MacKerell AD, Jr, Banavali N, Foloppe N. 2000. Development and current status of the CHARMM force field for nucleic acids. *Biopolymers* 56: 257–265. [https://doi.org/10.1002/1097-0282\(2000\)56:4<257::AID-BIP10029>3.0.CO;2-W](https://doi.org/10.1002/1097-0282(2000)56:4<257::AID-BIP10029>3.0.CO;2-W).
51. Zhang T, Nguyen PH, Nasica-Labouze J, Mu Y, Derreumaux P. 2015. Folding atomistic proteins in explicit solvent using simulated tempering. *J Phys Chem B* 119:6941–6951. <https://doi.org/10.1021/acs.jpcc.5b03381>.
52. Hoang Viet M, Derreumaux P, Nguyen PH. 2015. Communication: mul-

- multiple atomistic force fields in a single enhanced sampling simulation. *J Chem Phys* 143:e021101. <https://doi.org/10.1063/1.4926535>.
53. Lindorff-Larsen K, Piana S, Dror RO, Shaw DE. 2011. How fast-folding proteins fold. *Science* 334:517–520. <https://doi.org/10.1126/science.1208351>.
54. Jorgensen WL, Chandrasekhar J, Madura JD, Impey RW, Klein ML. 1998. Comparison of simple potential functions for simulating liquid water. *J Chem Phys* 79:926.
55. Darden T, York D, Pedersen L. 1993. Particle mesh Ewald: an $N\log(N)$ method for Ewald sums in large systems. *J Chem Phys* 98:10089–10092. <https://doi.org/10.1063/1.464397>.
56. Heussen C, Dowdle EB. 1980. Electrophoretic analysis of plasminogen activators in polyacrylamide gels containing sodium dodecyl sulfate and copolymerized substrates. *Anal Biochem* 102:196–202. [https://doi.org/10.1016/0003-2697\(80\)90338-3](https://doi.org/10.1016/0003-2697(80)90338-3).
57. Alves CR, Marzochi MC, Giovanni-de-Simone S. 1993. Heterogeneity of cysteine proteinases in *Leishmania braziliensis* and *Leishmania major*. *Braz J Med Biol Res* 26:167–171.
58. Monteerarat Y, Sakabe S, Ngamurulert S, Srichatraphimuk S, Jiamtom W, Chaichuen K, Thitithanyanont A, Permpikul P, Songserm T, Puthavathana P, Nidom CA, Mai Le Q, Iwatsuki-Horimoto K, Kawaoka Y, Auewarakul P. 2010. Induction of TNF-alpha in human macrophages by avian and human influenza viruses. *Arch Virol* 155:1273–1279. <https://doi.org/10.1007/s00705-010-0716-y>.